SCIENCE CHINA
Information Sciences

• RESEARCH PAPER •

March 2017, Vol. 60 032203:1–032203:14
doi: 10.1007/s11432-016-0169-8

$\mathcal{L}_1$ adaptive control of a generic hypersonic vehicle model with a blended pneumatic and thrust vectoring control strategy

Qi CHEN[1]*, Jing WAN[1] & Jianliang AI[1,2]

[1]*Department of Aeronautics and Astronautics, Fudan University, Shanghai* 200433*, China;*
[2]*Institute of Vehicle Design, Fudan University, Shanghai* 200433*, China*

Received April 22, 2016; accepted June 13, 2016; published online December 9, 2016

Abstract The extreme aeroheating at hypersonic regime and the insufficient dynamic pressure in the near space limit the achievable performance of the hypersonic vehicles using aerosurfaces alone. In this paper, an integrated pneumatic and thrust vectoring control strategy is employed to design a control scheme for the longitudinal dynamics of a hypersonic vehicle model. The methodology reposes upon a division of the model dynamics, and an $\mathcal{L}_1$ adaptive control architecture is applied to the design of the inner-loop and outer-loop controllers. Further, a control allocation algorithm is developed to coordinate pneumatic and thrust vectoring control. Simulation results demonstrate that the allocation algorithm is effective in control coordination, and the proposed control scheme achieves excellent tracking performance in spite of aerodynamic uncertainties.

Keywords hypersonic flight control, $\mathcal{L}_1$ adaptive control, thrust vectoring, control allocation, parametric uncertainty

Citation Chen Q, Wan J, Ai J L. $\mathcal{L}_1$ adaptive control of a generic hypersonic vehicle model with a blended pneumatic and thrust vectoring control strategy. Sci China Inf Sci, 2017, 60(3): 032203, doi: 10.1007/s11432-016-0169-8

1 Introduction

Hypersonic flight has been an intriguing field since roughly a century ago [1], and with the prospects of reliable and cost-effective access to space and the potential for prompt global strike capability, ongoing experimental and study efforts are being made throughout the aerospace community towards the goal of feasible and efficient hypersonic flights [2].

In 2011, two test flights under DARPA's Falcon Project ended unsuccessfully during the glide phase, indicating that conventional control techniques appropriate for subsonic and supersonic flights were not necessarily applicable for hypersonic flight [3]. The challenges of hypersonic flight control lie in limited wind tunnel data, poorly known physical models, and the harsh and uncertain operating conditions [4]. Furthermore, the large flight envelope which involves the variations in aerodynamics, thrust level, and vehicle mass along the flight trajectory also contributes to the control relevant challenges [5].

In combating theses challenges, numerous control architectures and methodologies have been proposed. While earlier work focused primarily on developing linear robust control laws for linearized hypersonic

* Corresponding author (email: qichen13@fudan.edu.cn)

models [6–8], recent years have seen a shift of attention to the design of nonlinear controllers for nonlinear vehicle models [9–13]. In [14], a nonlinear-disturbance-observer-based control method was adopted to improve robustness and disturbance rejection performance under mismatched disturbances. Under the back-stepping scheme, Xu et al. introduced an adaptive Kriging controller with the nominal feedback included in the controller and the Kriging system augmented to estimate the uncertainty [15]. A tracking-control strategy was proposed [16] based on using rather than cancelling aero-propulsive and elevator-to-lift couplings to deal with issues of couplings and non-minimum phase characteristics. In [13], a tracking differentiator was designed to reconstruct the angle of attack and flight path angle, both of which are difficult to measure in practice. In [17], Huang et al. introduced H_2 and H_∞ robustness into the well-known characteristic model-based golden-section adaptive control law, and designed a robust attitude control scheme for hypersonic cruise vehicles subject to external disturbances and aerodynamic uncertainties. Su et al. [18] integrated the input shaping technique and the constrained adaptive back-stepping control method for constrained adaptive tracking and elastic vibration control of a flexible hypersonic vehicle model. A discrete controller was proposed by Zhi et al. [19] with neural networks and backstepping technique, where the neural networks were adopted to estimate the unknown dynamics. Recently, a novel active robust control scheme was proposed by Pu et al. [20], which differed from the existing robust methodologies in that it used active approaches rather than inherent system robustness to simultaneously suppress diverse uncertainties and flexible modes.

This paper introduces an $\mathcal{L}_1$ adaptive controller with integrated pneumatic and thrust vectoring control that aims to control the longitudinal dynamics of a hypersonic vehicle model in the presence of aerodynamic uncertainties.

For the large envelope of a hypersonic vehicle, the air density in the atmosphere decreases as the altitude increases. When the vehicle enters the near space, the resultant low dynamic pressure would make the desired torque unattainable using aerodynamic surfaces alone [21]. A conventional approach is the incorporation of a reaction control system (RCS) which consists of thrusts that fire to produce rolling, pitching, and yawing moments [22]. Two schemes have been proposed, (1) hybrid control with aerodynamic surfaces and reaction control system [21, 23], and (2) the RCS alone provides the required moments [22]. However, the RCS has the following limitations: (1) only discrete control torque is available, which would lead system state trajectories to limit cycle behaviors; (2) the magnitude of the control moments are strictly constrained, thus limiting the achievable control performance; (3) frequent cycling of the RCS thrusters results in excessive wear on the RCS propellant control valves; and (4) the implementation of the RCS leads to a reduction in the payload. Another issue is that when the vehicle enters the hypersonic regime, it is subject to extreme aeroheating. Therefore, additional thermal coatings on the control surfaces are required, and deflection angels of aerodynamic surfaces are limited to avoid performance degradation [1, 18]. This work addresses the aforementioned issues by proposing a blended pneumatic and thrust vectoring control strategy. Thrust vector control spurs an increasing interest in aerospace community since enhanced maneuverability of the vehicle, which is appealing for an airbreathing hypersonic aircraft, can be achieved without the excessive need for high-strength nozzle materials. In addition, it has been verified on fighter planes as Su-30 MKI, F-22, JSF MIG-29 OVT and F-35 A/B/C [24]. Previously, Wang et al. [25] proposed a control scheme that applied the thrust vectoring technique in hypersonic flight control. However, two vector nozzles were required, and the nozzle deflection angles were fixed, thus restraining the control efficiency. In this work, the vector nozzle is rotatable and only limited by the deflection angle limits. And a control allocation algorithm is developed to calculate the deflection angles of the elevators and the thrust nozzle.

Since $\mathcal{L}_1$ adaptive control method is used to develop the control scheme, a brief summary of this methodology and its antecedent, adaptive control, is outlined next.

Adaptive control has been investigated in the research field of flight control since the mid 1950s. It requires less modelling information than classical robust controllers, and it is able to improve the performance in case of system uncertainties, parametric variations, and failures, thus making it a potential solution to the problem of hypersonic control [26]. A number of adaptive controllers have been designed for hypersonic flight [2, 4, 9, 10, 15, 18, 26]. Fiorentini et al. [10] adopted a combination of nonlinear sequential loop closure and adaptive dynamic inversion to design a nonlinear robust adaptive controller. The proposed method considered the effect of both parametric model uncertainty and dynamic perturbations due to flexible dynamics on stability robustness. In [4], Daniel et al. made adaptive augmentation to a gain-scheduled baseline LQR-PI controller and applied it to a 6-DOF hypersonic vehicle model. The model included uncertainty in control effectiveness, longitudinal center of gravity location, aerodynamic coefficients, sensor bias and noise, and input time delays. Two model reference adaptive augmentation setups were investigated: a classical open-loop reference model design, and a modified closed-loop reference model design. Simulation results demonstrated that while both augmentation configurations achieved better performance than the baseline controller, the closed-loop reference model design provided the best performance in the presence of uncertainties.

Despite its wide applications, conventional adaptive controllers are also identified with another characteristic that an increase in performance usually leads to a decrease in robustness properties, hence posing a challenge in finding a suitable trade-off [27, 28]. First proposed by Hovakimyan and Cao, $\mathcal{L}_1$ adaptive control architecture seeked to tackle the problem by decoupling adaptation from robustness. This design philosophy resulted in the achievement of guaranteed transient performance and robustness in the presence of fast adaptation [28]. In the field of hypersonic flight control, various attempts have been made to incorporate the $\mathcal{L}_1$ adaptive control architecture. Lei et al. [29] designed an $\mathcal{L}_1$ adaptive controller for Bolender and Doman's model in the presence of parametric uncertainties and unmodeled dynamics. Prime et al. [30] presented a full $\mathcal{L}_1$ adaptive controller, where the longitudinal flight dynamics of a waverider-class hypersonic vehicle was considered. The robustness of the controller was verified through various failure modes and modelling error simulations. In [31], the descent longitudinal trajectory control problem was studied by Banerjee et al. where the $\mathcal{L}_1$ adaptive controller was augmented to a dynamic pole placement controller to cancel out the matched uncertainties, and an enhancement to the control performance was proved by the simulations.

This paper is organized as follows: Section 2 introduces the vehicle model. In Section 3, the control development is presented: the control architecture is outlined, the inner-loop and outer-loop controllers are developed, and the control allocation algorithm is provided. Section 4 presents the simulation results, whereas final remarks are offered in Section 5.

2 Hypersonic vehicle model

The generic hypersonic vehicle model developed at NASA Langley Research Center is employed in this paper [9]. To incorporate thrust vectoring control, the set of equations depicting the longitudinal dynamics of the vehicle model is rewritten as follows:

$$\begin{aligned}&\dot{V}=\frac{T\cos(\alpha+\phi)-D}{m}-\frac{\mu\sin\gamma}{r^2},\quad \dot{\gamma}=\frac{L+T\sin(\alpha+\phi)}{mV}-\frac{(\mu-V^2r)\cos\gamma}{Vr^2},\\&\dot{h}=V\sin\gamma,\quad \dot{\alpha}=q-\dot{\gamma},\quad \dot{q}=\frac{M_{yy}}{I_{yy}},\end{aligned}\tag{1}$$

where

$$\begin{aligned}&L=\frac{1}{2}\rho V^2SC_{\mathrm{L}},\quad D=\frac{1}{2}\rho V^2SC_{\mathrm{D}},\quad T=\frac{1}{2}\rho V^2SC_{\mathrm{T}},\\&M_{yy}=\frac{1}{2}\rho V^2S\bar{c}\left[C_{\mathrm{M}}(\alpha)+C_{\mathrm{M}}(\delta_{\mathrm{e}}=0)+C_{\mathrm{M}}(q)\right]+\Delta M,\\&\Delta M=\frac{1}{2}\rho V^2S\bar{c}c_e\delta_{\mathrm{e}}+Tl\sin(\phi),\quad r=h+R_{\mathrm{E}}.\end{aligned}\tag{2}$$

The definition of the variables are listed as follows: V denotes the velocity of the vehicle, γ denotes the flight path angle, h denotes the altitude, α is the angle of attack, and q denotes the pitch rate; L, D, and T denote the lift, drag and thrust, with C_{L}, C_{D}, and C_{T} being the lift, drag and thrust coefficients; M_{yy} denotes the pitching moment, ΔM represents the moment generated by elevator deflection and thrust vectoring; $C_{\mathrm{M}}(\delta_{\mathrm{e}}=0)$ represents the moment coefficient contributed by elevator at zero deflection angle, and $C_{\mathrm{M}}(\alpha)$, $C_{\mathrm{M}}(q)$ are moment coefficients due to angle of attack and pitch rate, respectively. I_{yy} is the moment of inertia about the y axis, m denotes the mass of the vehicle, S denotes the reference area, $\bar{c}$ denotes the mean aerodynamic chord and c_e is the elevator coefficient. ϕ denotes the thrust nozzle deflection angle (a downward deflection is defined as positive) and l denotes the distance between the thrust nozzle and the vehicle gravity center. μ is the gravitational constant, R_{E} is the radius of the Earth and r denotes the radial distance from the center of the Earth. All variables listed above are defined in SI units.

The density of air ρ is modeled as a function of the altitude [32]:

$$\rho = 1.2266\mathrm{e}^{-\frac{h}{7315.2}}. \tag{3}$$

The engine dynamics is modeled as a second-order system:

$$\ddot{\beta} = -2\zeta\omega_{\mathrm{n}}\dot{\beta} - \omega_{\mathrm{n}}^2\beta + \omega_{\mathrm{n}}^2\beta_{\mathrm{c}}, \tag{4}$$

where β is the throttle setting, β_{c} is the commanded value, and ω_{n} and ζ are the natural frequency and damping ratio for the β dynamics, respectively.

The aerodynamic coefficients are approximated around a trimmed cruising condition ($V = 4590.28$ m/s, $h = 33528$ m, $\gamma = 0$ rad, and $q = 0$ rad/s) as follows:

$$\begin{aligned}
&C_{\mathrm{L}} = 0.6203\alpha,\\
&C_{\mathrm{D}} = 0.6450\alpha^2 + 0.0043378\alpha + 0.003772,\\
&C_{\mathrm{T}} = \begin{cases} 0.02576\beta, & \text{if} \quad \beta < 1,\\ 0.0224 + 0.00336\beta, & \text{if} \quad \beta > 1, \end{cases}\\
&C_{\mathrm{M}}(\alpha) = -0.035\alpha^2 + 0.036617\alpha + 5.3261 \times 10^{-6},\\
&C_{\mathrm{M}}(q) = \frac{q\bar{c}}{2V}(-6.796\alpha^2 + 0.3015\alpha - 0.2289),\\
&C_{\mathrm{M}}(\delta_{\mathrm{e}} = 0) = c_e(\delta_{\mathrm{e}} - \alpha)|_{\delta_{\mathrm{e}}=0} = -c_e\alpha.
\end{aligned} \tag{5}$$

The state of the system is $x_{hv} = [V, h, \alpha, \gamma, q]^{\mathrm{T}}$, and the control input is $u_{hv} = [\beta_{\mathrm{c}}, \delta_{\mathrm{e}}, \phi]^{\mathrm{T}}$. In this paper, the system output is chosen as $y_{hv} = [V, \gamma]^{\mathrm{T}}$. Additional details on the model can be found in [9].

3 Control development

This section presents the methodologies and strategies adopted in the control design. First the architecture of the control scheme is determined upon an examination of the system dynamics. Thereafter, the inner-loop and outer-loop controllers are designed with the $\mathcal{L}_1$ adaptive control method. Further, a control allocation algorithm is developed to coordinate pneumatic and thrust vectoring control.

3.1 Control architecture

The system given by (1) could be divided into three subsystems [29, 33].

The first consists of the pitch angle and the pitch rate:

$$\dot{\theta} = q, \quad \dot{q} = \frac{M_{yy}}{I_{yy}}. \tag{6}$$

It could be rewritten as

$$\begin{pmatrix} \dot{\theta} \\ \dot{q} \end{pmatrix} = \begin{bmatrix} 0 & 1 \\ M_\theta & M_q \end{bmatrix} \begin{pmatrix} \theta \\ q \end{pmatrix} + \begin{pmatrix} 0 \\ 1 \end{pmatrix} (\Delta M' + M^*), \tag{7}$$

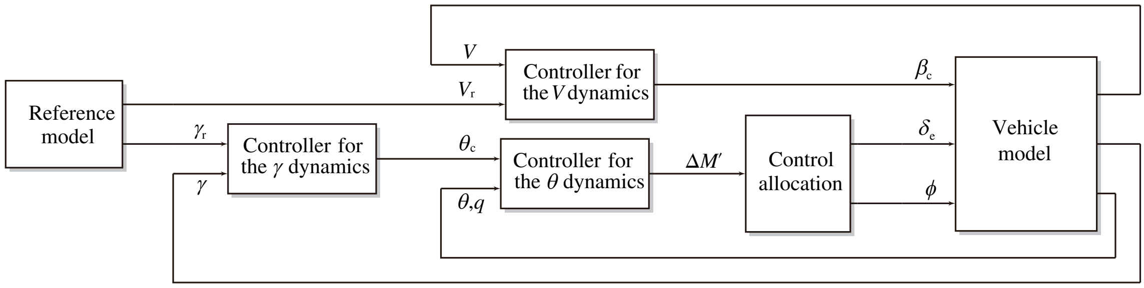

Figure 1 Conceptual block diagram of the proposed control scheme.

where

$$
\begin{aligned}
&M_\theta = 0, \quad M_q = \frac{\rho V S \bar{c}^2}{4I_{yy}}(-6.796\alpha^2 + 0.3015\alpha - 0.2289), \\
&\Delta M' = \frac{\Delta M}{I_{yy}}, \quad M^* = \frac{\rho V^2 S \bar{c}}{2I_{yy}}\left[C_{\rm M}(\alpha) + C_{\rm M}(\delta_{\rm e} = 0)\right].
\end{aligned} \tag{8}
$$

The second includes the flight path angle:

$$
\dot{\gamma} = \frac{L + T\sin(\alpha+\phi)}{mV} - \frac{(\mu - V^2 r)\cos\gamma}{Vr^2} = -\frac{T}{mV}\gamma + \frac{T}{mV}\theta + \sigma_\gamma, \tag{9}
$$

where

$$
\sigma_\gamma = \frac{L + T\sin(\alpha+\phi)}{mV} - \frac{(\mu - V^2 r)\cos\gamma}{Vr^2} + \frac{T}{mV}\gamma - \frac{T}{mV}\theta. \tag{10}
$$

And the third has the vehicle velocity:

$$
\dot{V} = \frac{T\cos(\alpha+\phi) - D}{m} - \frac{\mu\sin\gamma}{r^2}. \tag{11}
$$

Since the control objective is to ensure that the output y_{hv} tracks the reference trajectories of flight path angle and velocity, the second and third subsystems form the outer-loop, and controllers are required to generate the control inputs $\theta_{\rm c}$ (virtual control input) and $\beta_{\rm c}$. The inner-loop consists of the pitch dynamics, and an inner-loop controller is needed to generate the required pitching moment. Further, an allocation block is developed to produce the control inputs $\delta_{\rm e}$ and ϕ, which completes the control loop. A schematic representation of the overall control architecture is provided in Figure 1.

3.2 $\mathcal{L}_1$ adaptive controllers

This section presents the $\mathcal{L}_1$ adaptive control methodology employed to develop the controllers. The philosophy behind the controllers is that the nonlinearities are treated as bounded uncertain perturbations, and the $\mathcal{L}_1$ adaptive control technique is utilized to obtain a state feedback controller that estimates the uncertainties, as well as compensating for the uncertainties within the bandwidth of a predesigned low-pass filter [31]. A conceptual block diagram of the control scheme is provided in Figure 2.

Several assumptions are made before applying the $\mathcal{L}_1$ adaptive control technique [28, 31]. (1) uniform boundedness of the uncertainties $f(t, 0)$; (2) existence of semiglobal uniform boundedness of the partial derivatives of $f_i(t, 0)$; (3) stability of the unmodeled dynamics; and (4) partial knowledge of actuator dynamics $F_i(s)$.

3.2.1 *Inner-loop controller*

Consider again the dynamics given by (7), it could be cast into the following form:

$$
\dot{x} = A_{m,\theta}x + b_\theta\left[\Delta M' + (M_\theta - e_1)\theta + (M_q - e_2)q + M^*\right], \quad y = c_\theta^{\rm T}x, \tag{12}
$$

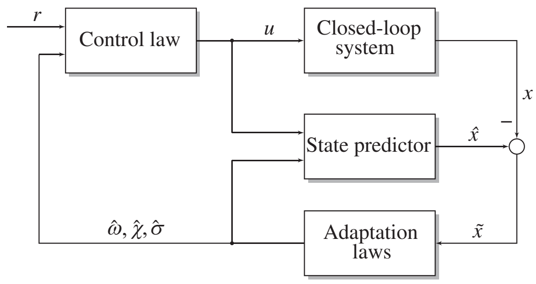

Figure 2 Interconnection of the $\mathcal{L}_1$ adaptive control scheme.

where $x = [\theta, q]^{\mathrm{T}}$ is the state of the system, $b_\theta = [0, 1]^{\mathrm{T}}$ is the input matrix, and $c_\theta = [1, 0]^{\mathrm{T}}$ is the output matrix,

$$A_{m,\theta} = \begin{bmatrix} 0 & 1 \\ e_1 & e_2 \end{bmatrix} \tag{13}$$

specifies the desired closed-loop dynamics and the variables are set as $e_1 = -1.3$, $e_2 = -1.8$ in this study. $\Delta M'(s) = F_M(s)\Delta M_{\mathrm{c}}(s)$, with $F_M(s) = 1$ denoting the actuator dynamics of the virtual input $\Delta M'$ and ΔM_{c} being the commanded value.

The control objective is to use the virtual input $\Delta M'$ to ensure that the pitch angle θ tracks the value commanded by the outer-loop.

For the problem formulated above, the following state predictor is considered:

$$\dot{\hat{x}}(t) = A_{m,\theta}\hat{x}(t) + b_\theta \left[\hat{\omega}_\theta(t)\Delta M_{\mathrm{c}}(t) + \hat{\chi}_\theta(t)||x_t||_{\mathcal{L}_\infty} + \hat{\sigma}_\theta(t)\right], \quad \hat{x}(0) = x_0, \tag{14}$$

where $\hat{x}(t)$ is the predicted state, $||x_t||_{\mathcal{L}_\infty}$ is the $\mathcal{L}_\infty$-norm of x, and the adaptive estimates $\hat{\omega}_\theta(t)$, $\hat{\chi}_\theta(t)$, $\hat{\sigma}_\theta(t) \in \mathbb{R}$ are calculated from the following projection-based adaptation laws:

$$\begin{aligned}
\dot{\hat{\omega}}_\theta(t) &= \Gamma_\theta \mathrm{Proj}\left(\hat{\omega}_\theta(t), -\tilde{x}^{\mathrm{T}}(t)P_\theta b_\theta \Delta M_{\mathrm{c}}(t)\right), \quad \hat{\omega}_\theta(0) = \hat{\omega}_{\theta,0}, \\
\dot{\hat{\chi}}_\theta(t) &= \Gamma_\theta \mathrm{Proj}\left(\hat{\chi}_\theta(t), -\tilde{x}^{\mathrm{T}}(t)P_\theta b_\theta ||x_t||_{\mathcal{L}_\infty}\right), \quad \hat{\chi}_\theta(0) = \hat{\chi}_{\theta,0}, \\
\dot{\hat{\sigma}}_\theta(t) &= \Gamma_\theta \mathrm{Proj}\left(\hat{\sigma}_\theta(t), -\tilde{x}^{\mathrm{T}}(t)P_\theta b_\theta\right), \quad \hat{\sigma}_\theta(0) = \hat{\sigma}_{\theta,0},
\end{aligned} \tag{15}$$

where $\tilde{x}(t) \triangleq \hat{x}(t) - x(t)$ denotes the prediction error of the system state, $\Gamma_\theta \in \mathbb{R}^+$ is the adaptation rate, P_θ is the solution of the algebraic Lyapunov equation $A_{m,\theta}^{\mathrm{T}}P_\theta + P_\theta A_{m,\theta} = -Q_\theta$ for arbitrary symmetrical positive definite matrix Q_θ.

The control signal is the output of the feedback system presented below:

$$\Delta M_{\mathrm{c}}(s) = -k_\theta D_\theta(s)\left(\hat{\eta}_\theta(s) - k_{g,\theta}\theta_c(s)\right), \tag{16}$$

where $\theta_c(s)$ and $\hat{\eta}_\theta(s)$ are the Laplace transforms of the reference signal $\theta_c(t)$ and $\hat{\eta}_\theta(t) \triangleq \hat{\omega}_\theta(t)\Delta M_{\mathrm{c}}(t) + \hat{\chi}_\theta(t)||x_t||_{\mathcal{L}_\infty} + \hat{\sigma}_\theta(t)$, and $k_{g,\theta} \triangleq -1/\left(c_\theta^{\mathrm{T}} A_{m,\theta}^{-1} b_\theta\right)$. $k_\theta \in \mathbb{R}^+$ is a feedback gain and $D_\theta(s)$ is a strictly proper transfer function that brings forth a strictly proper stable

$$C_\theta(s) = \frac{k_\theta F_M(s) D_\theta(s)}{1 + k_\theta F_M(s) D_\theta(s)} \tag{17}$$

with $C_\theta(0) = 1$.

The $\mathcal{L}_1$ adaptive controller is defined via (14)–(16). To ensure the stability of the system, the following $\mathcal{L}_1$-norm condition needs to be met [28, 29]:

$$||G_\theta(s)||_{\mathcal{L}_1} L_\chi < 1, \tag{18}$$

where

$$L_\chi \triangleq \max||\chi_\theta||_1, \quad H_\theta(s) \triangleq (s\mathbb{I}_2 - A_{m,\theta})^{-1} b_\theta, \quad G_\theta(s) \triangleq H_\theta(s)\left(1 - C_\theta(s)\right). \tag{19}$$

The design parameters are selected as follows:

$$\Gamma_\theta = 150000, \quad k_\theta = 3, \quad D_\theta(s) = \frac{\omega_{c,\theta}^2(3s+\omega_{c,\theta})}{s(s+\omega_{c,\theta})^3}, \tag{20}$$

where $\omega_{c,\theta}$ is set as 6.

3.2.2 *Outer-loop controllers*

This section gives a brief introduction to the design of the controllers for the outer-loop.

The flight path angle dynamics presented in (9) could be written as follows:

$$\dot{\gamma} = A_{m,\gamma}\gamma + b_\gamma \left[\frac{T}{b_\gamma mV}\theta - \left(\frac{T}{b_\gamma mV} - \frac{A_{m,\gamma}}{b_\gamma}\right)\gamma + \frac{\sigma_\gamma}{b_\gamma}\right], \tag{21}$$

where $A_{m,\gamma} = -0.24$ is set to specify the desired closed-loop dynamics, $b_\gamma = 0.03$ is the input matrix. $\theta(s) = F_\theta(s)\theta_{\mathrm{c}}(s)$, where θ_{c} denotes the commanded value, and it follows from (13) that

$$F_\theta(s) = \frac{1.3}{s^2+1.8s+1.3}. \tag{22}$$

The control objective of the $\mathcal{L}_1$ adaptive controller for the flight path loop is to use the virtual control input θ to ensure that γ tracks the reference trajectory.

The following state predictor is considered:

$$\dot{\hat{\gamma}}(t) = A_{m,\gamma}\hat{\gamma}(t) + b_\gamma\left[\hat{\omega}_\gamma(t)\theta_{\mathrm{c}}(t) + \hat{\chi}_\gamma(t)||\gamma_t||_{\mathcal{L}_\infty} + \hat{\sigma}_\gamma(t)\right], \quad \hat{\gamma}(0) = \gamma_0, \tag{23}$$

where the adaptive estimates $\hat{\omega}_\gamma(t)$, $\hat{\chi}_\gamma(t)$, $\hat{\sigma}_\gamma(t)$ are calculated from the following adaptation laws:

$$\begin{aligned} \dot{\hat{\omega}}_\gamma(t) &= \Gamma_\gamma \mathrm{Proj}\left(\hat{\omega}_\gamma(t), -\tilde{\gamma}(t)P_\gamma b_\gamma \theta_{\mathrm{c}}(t)\right), \quad \hat{\omega}_\gamma(0) = \hat{\omega}_{\gamma,0}, \\ \dot{\hat{\chi}}_\gamma(t) &= \Gamma_\gamma \mathrm{Proj}\left(\hat{\chi}_\gamma(t), -\tilde{\gamma}(t)P_\gamma b_\gamma ||\gamma_t||_{\mathcal{L}_\infty}\right), \quad \hat{\chi}_\gamma(0) = \hat{\chi}_{\gamma,0}, \\ \dot{\hat{\sigma}}_\gamma(t) &= \Gamma_\gamma \mathrm{Proj}\left(\hat{\sigma}_\gamma(t), -\tilde{\gamma}(t)P_\gamma b_\gamma\right), \quad \hat{\sigma}_\gamma(0) = \hat{\sigma}_{\gamma,0}. \end{aligned} \tag{24}$$

The control signal is generated from the following feedback system:

$$\theta_{\mathrm{c}}(s) = -k_\gamma D_\gamma(s)\left(\hat{\eta}_\gamma(s) - k_{g,\gamma}\gamma_r(s)\right). \tag{25}$$

The design parameters are chosen as below:

$$\Gamma_\gamma = 120000, \quad k_\gamma = 12, \quad D_\gamma(s) = \frac{s^2+2s+5}{s^3+20s^2+200s}\frac{3\omega_{c,\gamma}^2 s + \omega_{c,\gamma}^3}{(s+\omega_{c,\gamma})^3}, \tag{26}$$

where $\omega_{c,\gamma}$ is set as 1.2.

For the velocity channel, similar procedures are taken to design the controller. The velocity dynamics could be cast into the following error dynamics:

$$\dot{V}_{\mathrm{e}} = A_{m,V}V_{\mathrm{e}} + b_V\left[\frac{1}{b_V m}\frac{\partial T}{\partial \beta}\beta - \left(\frac{2\mu\sin\gamma}{b_V r^2} + \frac{A_{m,V}}{b_V}\right)V_{\mathrm{e}} + \frac{\sigma_V}{b_V}\right], \tag{27}$$

where

$$\sigma_V = -\frac{1}{m}\frac{\partial T}{\partial \beta}\beta + \frac{2\mu\sin\gamma}{r^2}V_{\mathrm{e}} + \frac{T\cos(\alpha+\phi)-D}{m} - \frac{\mu\sin\gamma}{r^2} - \dot{V}_r, \tag{28}$$

and $A_{m,V} = -0.09$ is selected to specify the desired closed-loop dynamics, $b_V = 0.3$ is the input matrix; $V_{\mathrm{e}} = V - V_{\mathrm{r}}$ denotes the velocity error where V_{r} is the reference value. $\beta(s) = F_\beta(s)\beta_{\mathrm{c}}(s)$, where β_{c} is the commanded value, and it follows from (4) that

$$F_\beta(s) = \frac{\omega_{\mathrm{n}}^2}{s^2+2\zeta\omega_{\mathrm{n}}s+\omega_{\mathrm{n}}^2}. \tag{29}$$

The objective of the $\mathcal{L}_1$ adaptive controller for the velocity channel is to utilize the control input β to ensure that the velocity tracks the reference value during the transient and steady state.

The state predictor is presented as follows:

$$\dot{\hat{V}}_{\mathrm{e}}(t) = A_{m,V}\hat{V}_{\mathrm{e}}(t) + b_V\left[\hat{\omega}_V(t)\beta_{\mathrm{c}}(t) + \hat{\chi}_V(t)||V_{\mathrm{e},t}||_{\mathcal{L}_\infty} + \hat{\sigma}_V(t)\right], \quad \hat{V}_{\mathrm{e}}(0) = V_{\mathrm{e},0}, \tag{30}$$

where the adaptive estimates $\hat{\omega}_V(t)$, $\hat{\chi}_V(t)$, $\hat{\sigma}_V(t)$ are calculated from the following adaptation laws:

$$\begin{aligned}
\dot{\hat{\omega}}_V(t) &= \Gamma_V \mathrm{Proj}\left(\hat{\omega}_V(t), -\tilde{V}_{\mathrm{e}}(t)P_V b_V \beta_{\mathrm{c}}(t)\right), \quad \hat{\omega}_V(0) = \hat{\omega}_{V,0},\\
\dot{\hat{\chi}}_V(t) &= \Gamma_V \mathrm{Proj}\left(\hat{\chi}_V(t), -\tilde{V}_{\mathrm{e}}(t)P_V b_V ||V_{\mathrm{e},t}||_{\mathcal{L}_\infty}\right), \quad \hat{\chi}_V(0) = \hat{\chi}_{V,0},\\
\dot{\hat{\sigma}}_V(t) &= \Gamma_V \mathrm{Proj}\left(\hat{\sigma}_V(t), -\tilde{V}_{\mathrm{e}}(t)P_V b_V\right), \quad \hat{\sigma}_V(0) = \hat{\sigma}_{V,0}.
\end{aligned} \tag{31}$$

The control signal is generated from the following feedback system:

$$\beta_{\mathrm{c}}(s) = -k_V D_V(s)\left(\hat{\eta}_V(s) - k_{g,V}V_{\mathrm{r}}(s)\right). \tag{32}$$

The design parameters are set as below:

$$\Gamma_V = 30000, \quad k_V = 0.1, \quad D_V(s) = \frac{1}{s}. \tag{33}$$

This section offers a brief introduction to the $\mathcal{L}_1$ adaptive controller applied in this research. Detailed account on the methodology, the proof of stability and the derivation of performance bounds could be found in [28].

3.3 Control allocation

The inner loop controller presented in Subsection 3.2.1 generates the required moment to achieve flight path tracking, however, the command value for the deflection angle of the elevators and the thrust nozzle are not determined. In this section, a control allocation algorithm is developed to coordinate pneumatic and thrust vectoring control.

Following (8), the pitching moment is given as

$$\Delta M = I_{yy}\Delta M'. \tag{34}$$

Denoting by $\kappa \in [0,1]$ the contribution that thrust vectoring control makes, the following expressions give the command value of deflection angle of the thrust nozzle and the elevators:

$$\phi = \arcsin\left(\frac{\Delta M\kappa}{Tl}\right), \quad \delta_{\mathrm{e}} = \frac{2\Delta M(1-\kappa)}{\rho V^2 S\bar{c}c_e}. \tag{35}$$

During the flight, the value of κ could be held constant during one flight phase, or changed from one phase to another. For example, to decrease the thermal loads on the control surfaces, or when the control surfaces alone are unable to serve the control purpose, a larger value of κ could be designated. To ensure smooth transition between different modes, the signal of κ is filtered via the following filter:

$$F_p(s) = \frac{\omega_{p1}}{s+\omega_{p1}}\frac{\omega_{p2}^2}{s^2+2\epsilon_p\omega_{p2}s+\omega_{p2}^2} \tag{36}$$

with the following values assigned:

$$\omega_{p1} = 1, \quad \omega_{p2} = 0.2, \quad \epsilon_p = 1. \tag{37}$$

This control allocation algorithm could be implemented with an onboard computation block that uses system state V, control signal β_{c} and, $\Delta M'$ as the inputs and generate the control signals ϕ and δ_{e} as the the outputs. The choice of the value for κ which depends on the needs for thermal protection of the control surfaces and the level of maneuverability required in different flight conditions, is beyond the scope of current work. However, borrowing from the philosophy of gain-schedule control, a scheduled κ setting may provide a practical solution for the large envelope of a hypersonic vehicle.

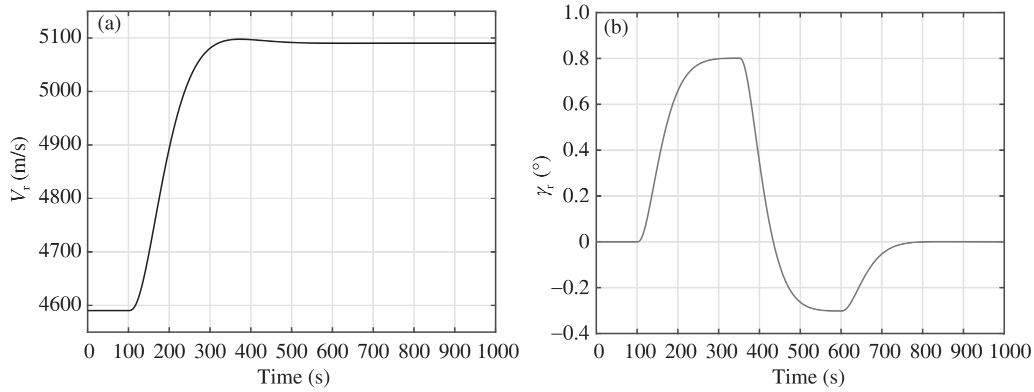

Figure 3 Reference trajectories. (a) $V_{\rm r}$; (b) γ_r.

Table 1 Bounds of the uncertain aerodynamic coefficients

Element of error vector	Error bounds (3σ limits)
$\epsilon_{C_{\rm L}^{\alpha}}$	$[0.745, 1.255]$
$\epsilon_{C_{\rm D}^{\alpha}}$	$[0.88, 1.12]$
$\epsilon_{C_{\rm M}^{\alpha}}$	$[0.85, 1.15]$
$\epsilon_{C_{\rm M}^{q}}$	$[0.475, 1.525]$
$\epsilon_{C_{\rm M}^{\delta_{\rm e}}}$	$[0.925, 1.075]$

4 Simulations

4.1 Simulation scenarios

Simulations are performed to validate the control scheme developed in the previous sections. Two representative case studies will be presented: the first test case examines the performance of the proposed controller in different control modes (with different values of κ assigned), while in the second test case, the effectiveness of the controller under mode transition is verified.

The trimmed cruising condition of $h = 33528$ m and $V = 4590.28$ m/s is used as the initial condition of the simulation. The hypersonic vehicle model is expected to track a step change of $+500$ m/s in velocity at time $t = 100$ s, and meanwhile follow step changes of $+0.8^\circ$, -1.1° and $+0.3^\circ$ in flight path angle at $t = 100$ s, $t = 350$ s, and $t = 600$ s, respectively. The reference trajectories of velocity and flight path angle are generated via the following filters [34]:

$$F_V(s) = \frac{\omega_{c1}}{s+\omega_{c1}} \frac{\omega_{c2}^2}{s^2+2\epsilon_{c1}\omega_{c2}s+\omega_{c2}^2}, \tag{38}$$

$$F_\gamma(s) = \frac{\omega_{c3}}{s+\omega_{c3}} \frac{\omega_{c4}^2}{s^2+2\epsilon_{c2}\omega_{c4}s+\omega_{c4}^2}, \tag{39}$$

with the following values assigned:

$$\omega_{c1} = 0.1, \quad \omega_{c2} = 0.02, \quad \epsilon_{c1} = 0.8; \tag{40}$$

$$\omega_{c3} = 0.2, \quad \omega_{c4} = 0.03, \quad \epsilon_{c2} = 0.9. \tag{41}$$

The reference trajectories are depicted in Figure 3. It could be seen from the flight path angle plot that the vehicle model is expected to fly along both ascending and descending trajectories.

To assess the robustness of the proposed control scheme, time-varying uncertainties of the aerodynamic coefficients are introduced in both test cases, as presented in Table 1. The uncertain aerodynamic variables comprise the lift coefficient, the drag coefficient, the longitudinal stability of the model, the pitch damping, and the elevator pitching moment derivative. The uncertainties of the coefficients can be combined into

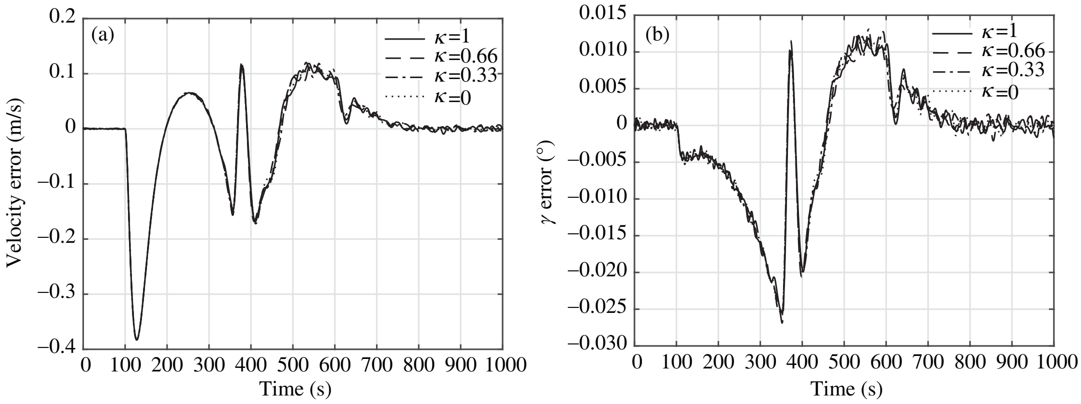

Figure 4 Tracking errors of the proposed control scheme. (a) Tracking error $V - V_{\mathrm{r}}$; (b) tracking error $\gamma - \gamma_r$.

the following vector:

$$e = \left[\epsilon_{C_{\mathrm{L}}^{\alpha}}, \epsilon_{C_{\mathrm{D}}^{\alpha}}, \epsilon_{C_{\mathrm{M}}^{\alpha}}, \epsilon_{C_{\mathrm{M}}^{q}}, \epsilon_{C_{\mathrm{M}}^{\delta_{\mathrm{e}}}}\right]^{\mathrm{T}}, \tag{42}$$

where each element denotes the multiplicative uncertainties of the coefficients with unity nominal values [35]. The values of each element obeys a continuous normal distribution and the three sigma limits.

4.2 Validation of the proposed control scheme

Simulation results demonstrate the performance of the proposed controller. As seen in Figure 4, the tracking error of both controlled outputs remains substantially small throughout the entire maneuver, and asymptotic convergence can be observed. Notably, the velocity error is several orders smaller than that of the velocity reference command, and the flight path tracking error remains within 3.5% of the magnitude of the reference trajectory. Concerning the fact that flight path angle γ is indirectly controlled by pitch angle θ, the tracking performance achieved is remarkably good. Furthermore, the tracking performance is retained with the change in allocation parameter κ, which validates the effectiveness of the controller in different control modes.

Figure 5 depicts the time history of the control inputs under the proposed control scheme. The relationship between the control effort and the allocation parameter κ is clearly shown by the plots: an increase in κ leads to more effort from thrust vectoring control and less effort from pneumatic control. Notice that the history of throttle setting remains the same with respect to all four κ settings, as expected from the control design. Mild oscillations are visible in Figures 5(b) and (c), revealing the control effort spent to combat the aerodynamic uncertainties. Overall, the control input behaviors remain stable and well behaved throughout the simulation phase, the effectiveness of the allocation algorithm and the capability of the proposed controller in the presence of uncertainties are confirmed.

4.3 Performance of the controller in mode transition

The second test case is designed to verify the effectiveness of the proposed control in mode transition. The value of the allocation parameter is initially set as $\kappa = 0.2$, and step changes of $+0.6$ and -0.3 are commanded at $t = 280$ s and $t = 550$ s, respectively.

Simulation is conducted without retuning the controller, and the same test trajectories used in the previous simulations are employed to simplify the comparison of the results. Figure 6 presents the tracking error behavior of the scheme in mode transition. Compared with Figure 4, the tracking performance is retained and the tracking error for both controlled variables remains substantially small.

The control inputs are plotted in Figures 7(a) and (b). Since the velocity dynamics are not affected by the change of the allocation parameter (as shown in Figure 5), the plot of the time history of throttle setting β is omitted here for reasons of space. Again, the control input behaviors remain stable and well behaved, and the mode transitions can be observed from the time history of δ_{e} and ϕ: beginning from $t = 280$ s, the thrust vectoring control spends more effort with an increase in the nozzle deflection angle

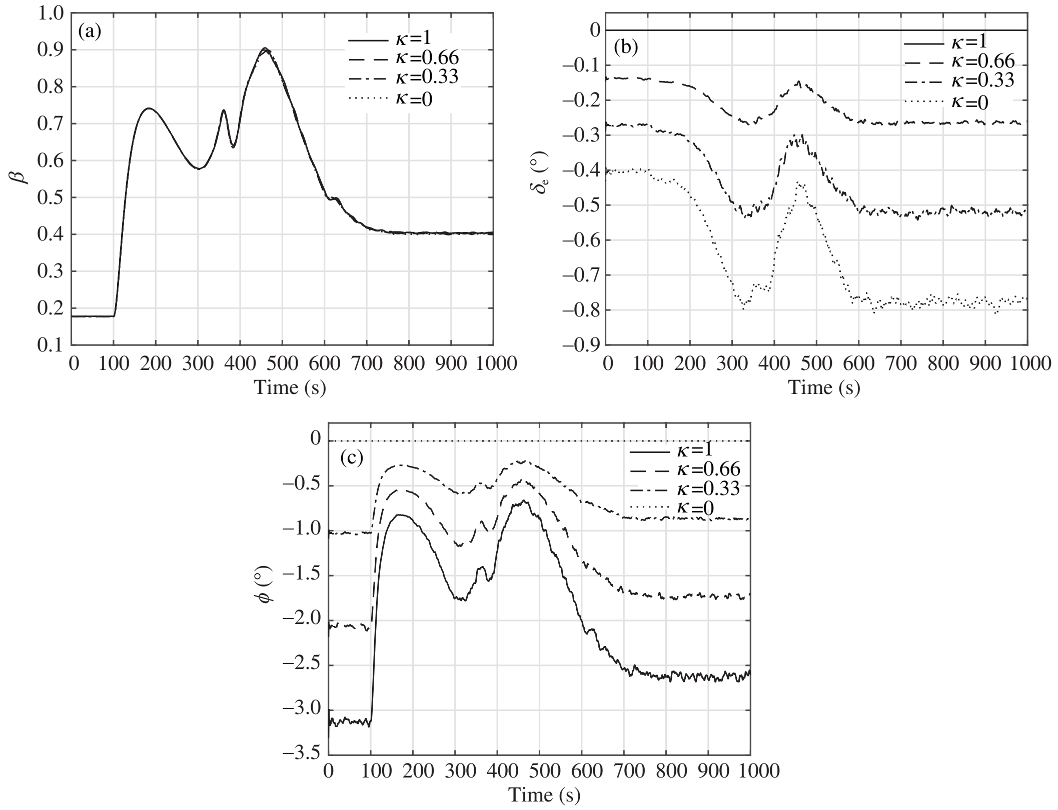

Figure 5 Control inputs of the proposed controller. (a) Control input β; (b) control input δ_{e}; (c) control input ϕ.

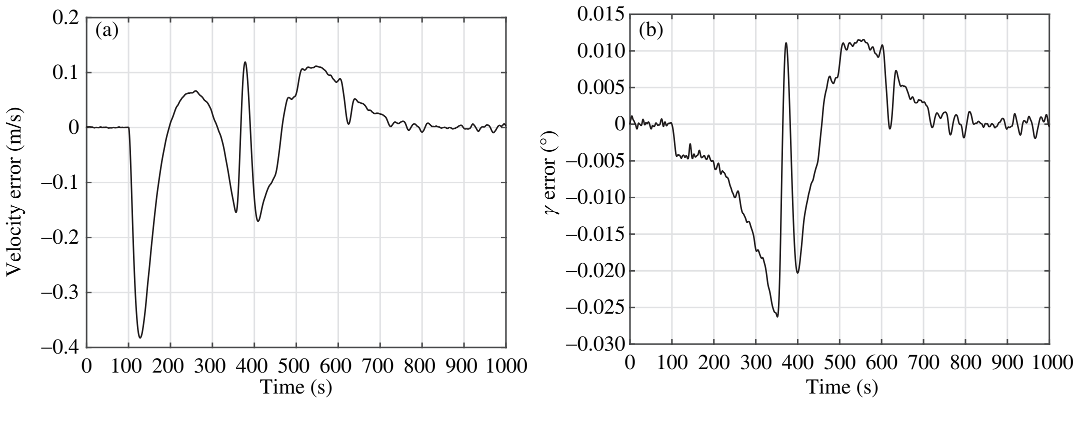

Figure 6 Tracking error plots. (a) V tracking error; (b) γ tracking error.

ϕ until at $t = 280$ s, an increase in the elevator deflection angle δ_{e} is seen with the decrease in κ. Angular states q and α of the vehicle model are shown in Figures 7(c) and (d). The oscillations in the pitch rate plot reveal the effect of the aerodynamic uncertainties. The time history of dynamic pressure and altitude is depicted in Figures 7(e) and (f). The effectiveness of the controller in mode transitions is validated by the second test case.

5 Conclusion

This paper presents a novel control methodology for a hypersonic vehicle model. The main focus is on the design of a control scheme that incorporates a combined pneumatic and thrust vectoring control strategy, while guaranteeing desired transient and steady-state performance in the presence of aerodynamic uncer-

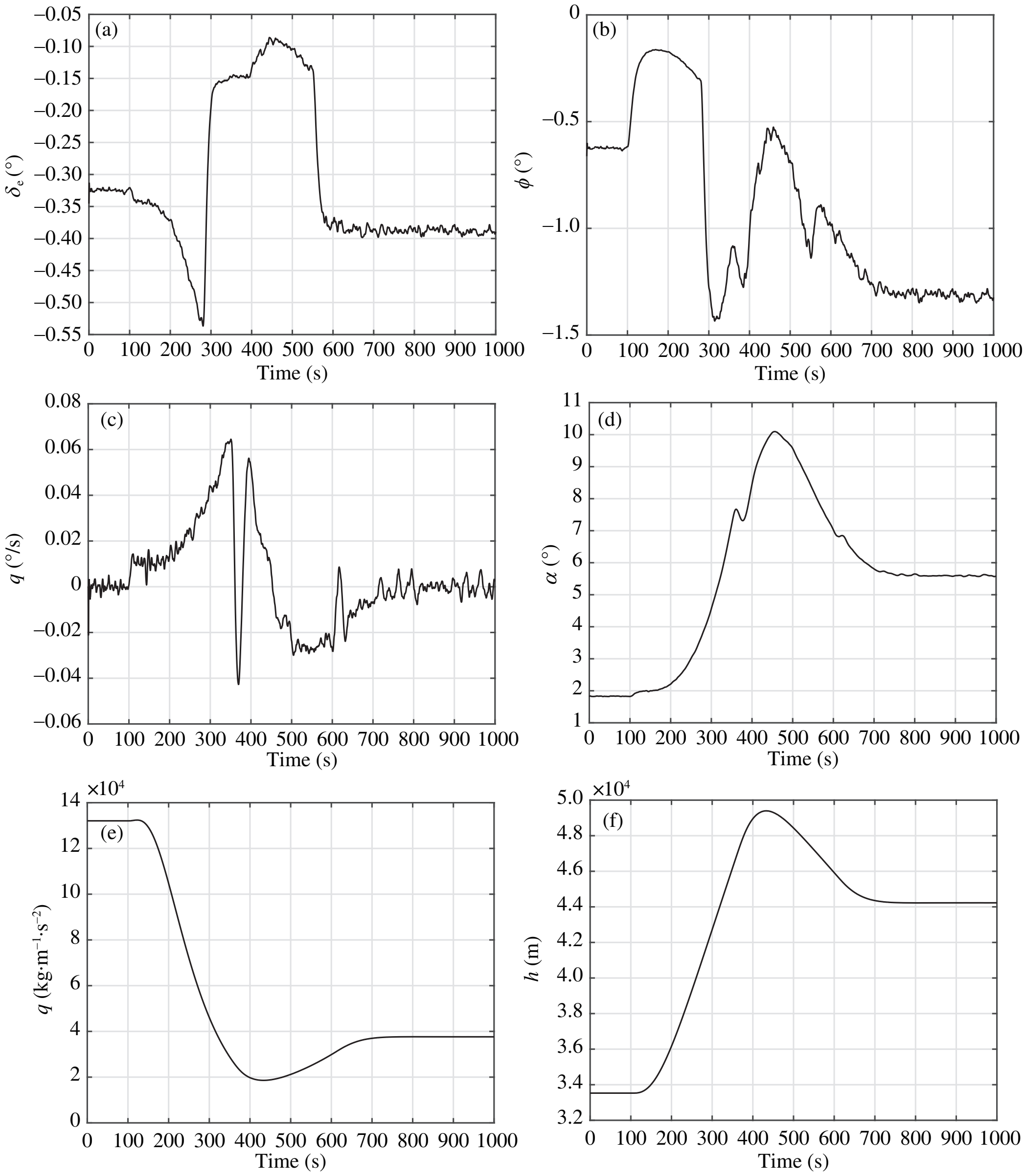

Figure 7 Simulation results of the second test case study. (a) Control input δ_e; (b) control input ϕ; (c) angular state q; (d) angular state α; (e) dynamic pressure $\bar{q}$; (f) altitude h.

tainties. The method reposes upon a division of the model dynamics and three $\mathcal{L}_1$ adaptive controllers are designed to achieve the control objective and compensate for the uncertainties. Thereafter, a control allocation algorithm is developed to determine the deflection angle of the elevators and the thrust nozzle. Combining the tracking error performance along with the behavior of control inputs from the simulation results of two test case studies, it is concluded that the proposed control scheme is successful in achieving guaranteed performance in the presence of uncertainties and the allocation algorithm is effective in control coordination. Future work will look to the investigation of techniques to extend the strategy to the whole flight envelop of a hypersonic vehicle model. The lateral dynamics will also be included to further extend the application of the methodology.

Conflict of interest The authors declare that they have no conflict of interest.

References

1 Hallion R. The history of hypersonics: or, 'Back to the future: again and again'. In: Proceedings of the 43rd AIAA Aerospace Sciences Meeting and Exhibit, Reno, 2005. AIAA 2005-329

2 Fiorentini L, Serrani A, Bolender M A, et al. Robust nonlinear sequential loop closure control design for an air-breathing hypersonic vehicle model. In: Proceedings of American Control Conference, Washington, 2008. 3458–3463

3 Christopher P, Morgan B, Ilya K. Model predictive control guidance with extended command governor inner-Loop flight control for hypersonic vehicles. In: Proceedings of AIAA Guidance, Navigation, and Control (GNC) Conference, Boston, 2013. AIAA 2013-5028

4 Daniel P W, Anuradha M A, Jonathan A M, et al. Adaptive control of a generic hypersonic vehicle. In: Proceedings of AIAA Guidance, Navigation, and Control (GNC) Conference, Boston, 2013. AIAA 2013-4514

5 Preller D, Smart M K. Longitudinal control strategy for hypersonic accelerating vehicles. J Spacecr Rockets, 2015, 52: 993–999

6 Buschek H, Calise A J. Uncertainty modeling and fixed-order controller design for a hypersonic vehicle model. J Guid Control Dyn, 1997, 20: 42–48

7 Chavez F R, Schmidt D K. Uncertainty modeling for multivariable-control robustness analysis of elastic high-speed vehicles. J Guid Control Dyn, 1999, 22: 87–95

8 Lind R. Linear parameter-varying modeling and control of structural dynamics with aerothermoelastic effects. J Guid Control Dyn, 2002, 25: 733–739

9 Xu H J, Mirmirani M D, Ioannou P A. Adaptive sliding mode control design for a hypersonic flight vehicle. J Guid Control Dyn, 2004, 27: 829–838

10 Fiorentini L, Serrani A, Bolender M A, et al. Nonlinear robust adaptive control of flexible air-breathing hypersonic vehicles. J Guid Control Dyn, 2009, 32: 402–417

11 Wilcox Z D, MacKunis W, Bhat S, et al. Lyapunov-based exponential tracking control of a hypersonic aircraft with aerothermoelastic effects. J Guid Control Dyn, 2010, 33: 1213–1224

12 Sun H B, Li S H, Sun C Y. Finite time integral sliding mode control of hypersonic vehicles. Nonlinear Dyn, 2013, 73: 229–244

13 Bu X W, Wu X Y, Zhang R, et al. Tracking differentiator design for the robust backstepping control of a flexible air-breathing hypersonic vehicle. J Frankl Inst-Eng Appl Math, 2015, 352: 1739–1765

14 Yang J, Li S H, Sun C Y, et al. Nonlinear-disturbance-observer-based robust flight control for air-breathing hypersonic vehicles. IEEE Trans Aerosp Electron Syst, 2013, 49: 1263–1275

15 Xu B, Sun F, Liu H, et al. Adaptive Kriging controller design for hypersonic flight vehicle via back-stepping. IET Contr Theory Appl, 2012, 6: 487–497

16 Sun H F, Yang Z L, Zeng J P. New tracking-control strategy for airbreathing hypersonic vehicles. J Guid Control Dyn, 2013, 36: 846–859

17 Huang H, Zhang Z. Characteristic model-based H_2/H_∞ robust adaptive control during the re-entry of hypersonic cruise vehicles. Sci China Inf Sci, 2014, 58: 1–21

18 Su X F, Jia Y M. Constrained adaptive tracking and command shaped vibration control of flexible hypersonic vehicles. IET Contr Theory Appl, 2015, 9: 1857–1868

19 Zhi Y, Yang Y. Discrete control of longitudinal dynamics for hypersonic flight vehicle using neural networks. Sci China Inf Sci, 2015, 58: 1–10

20 Pu Z Q, Yuan R Y, Tan X M, et al. Active robust control of uncertainty and flexibility suppression for air-breathing hypersonic vehicles. Aerosp Sci Tech, 2015, 42: 429–441

21 Geng J, Sheng Y Z, Liu X D. Finite-time sliding mode attitude control for a reentry vehicle with blended aerodynamic surfaces and a reaction control system. Chin J Aeronaut, 2014, 27: 964–976

22 Cai G H, Song J M, Chen X X. Command tracking control system design and evaluation for hypersonic reentry vehicles driven by a reaction control system. J Aerosp Eng, 2015, 28: 04014115

23 Cai G, Song J, Chen X. Control system design for hypersonic reentry vehicle driven by aerosurfaces and reaction control system. P I Mech Eng G-J Aer, 2014, 229: 1575–1587

24 Cen Z, Smith T, Stewart P, et al. Integrated flight/thrust vectoring control for jet-powered unmanned aerial vehicles with ACHEON propulsion. P I Mech Eng G-J Aer, 2014, 229: 1057–1075

25 Wang H L, Qin G Z, Wang Q Y, et al. Tracking control for a hypersonic air-breathing vehicle with thrust vectoring nozzles (in Chinese). Sci Sin-Phys Mech Astron, 2013, 43: 415–423

26 Poderico M, Morani G, Sollazzo A, et al. Fault-tolerant control laws against sensors failures for hypersonic flight. In: Proceedings of the 18th AIAA/3AF International Space Planes and Hypersonic Systems and Technologies Conference, Tours, 2012. AIAA 2012-5967

27 Hellmundt F, Wildschek A, Maier R, et al. Comparison of L1 adaptive augmentation strategies for a differential PI baseline controller on a longitudinal F16 aircraft model. In: Advances in Aerospace Guidance, Navigation and Control. Berlin: Springer, 2015. 99–118

28 Hovakimyan N, Cao C. L1 Adaptive Control Theory: Guaranteed Robustness With Fast Adaptation. Philadelphia: Society for Industrial and Applied Mathematics, 2010

29 Lei Y, Cao C, Cliff E, et al. Design of an L1 adaptive controller for air-breathing hypersonic vehicle model in the presence of unmodeled dynamics. In: Proceedings of AIAA Guidance, Navigation and Control Conference and Exhibit, Hilton Head, 2007. AIAA 2007-6527

30 Prime Z, Doolan C, Cazzolato B. Longitudinal L1 Adaptive control of a hypersonic re-entry experiment. In: Proceedings of the 15th Australian International Aerospace Congress (AIAC15), Melbourne, 2013. 717–726

31 Banerjee S, Wang Z, Baur B, et al. L1 Adaptive control augmentation for the longitudinal dynamics of a hypersonic glider. J Guid Control Dyn, 2015, 39: 275–291

32 Wang Q, Stengel R F. Robust nonlinear control of a hypersonic aircraft. J Guid Control Dyn, 2000, 23: 577–585

33 Tony A, Zhu J, Michael B, et al. Flight control of hypersonic scramjet vehicles using a differential algebraic approach. In: Proceedings of AIAA Guidance, Navigation, and Control Conference and Exhibit, Keystone, Colorado, 2006. AIAA 2006-6559

34 Xu B, Shi Z K, Yang C G, et al. Neural control of hypersonic flight vehicle model via time-scale decomposition with throttle setting constraint. Nonlinear Dyn, 2013, 73: 1849–1861

35 Banerjee S, Creagh M A, Boyce R R. L1 adaptive control augmentation configuration for a hypersonic glider in the presence of uncertainties. In: Proceedings of AIAA Guidance, Navigation, and Control Conference, National Harbor, Maryland, 2014. AIAA 2014-0453